

Copyright

by

Jacob Alexander Hummel

2012

The Thesis committee for Jacob Alexander Hummel
Certifies that this is the approved version of the following thesis:

**The Hunt for the First Supernovae:
The Source Density and Observability of Pair Instability
Supernovae from the First Stars**

**APPROVED BY
SUPERVISING COMMITTEE:**

Supervisor: _____
Volker Bromm

Miloš Milosavljević

**The Hunt for the First Supernovae:
The Source Density and Observability of Pair Instability
Supernovae from the First Stars**

by

Jacob Alexander Hummel, B.S.

Thesis

Presented to the Faculty of the Graduate School

of The University of Texas at Austin

in Partial Fulfillment

of the Requirements

for the Degree of

Master of Arts

The University of Texas at Austin

May 2012

Acknowledgments

I would first like to thank my advisor, Volker Bromm, for his guidance and encouragement throughout the writing of this thesis. I would also like to thank my committee: Miloš Milosavljević, J. Craig Wheeler, Eiichiro Komatsu and Karl Gebhardt. They have provided me with a great deal of valuable advice. The support and encouragement provided by my family and fellow graduate students has been invaluable throughout this process. I would especially like to thank my parents for fostering in me a thirst for knowledge and always encouraging my love of science. And most of all I would like to thank my fiancée, Sarah, for putting up with the years apart, the late nights, and the sleepless ones. Without her, none of this would have been possible.

JACOB ALEXANDER HUMMEL

The University of Texas at Austin

May 2012

**The Hunt for the First Supernovae:
The Source Density and Observability of Pair Instability
Supernovae from the First Stars**

by

Jacob Alexander Hummel, M.A.

The University of Texas at Austin, 2012

SUPERVISOR: Volker Bromm

Theoretical models predict that some of the first stars ended their lives as extremely energetic pair-instability supernovae (PISNe). With energies approaching 10^{53} ergs, these supernovae are expected to be within the detection limits of the upcoming *James Webb Space Telescope* (JWST), allowing observational constraints to be placed on the properties of the first stars. We estimate the source density of PISNe using a semi-analytic halo mass function based approach, accounting for the effects of feedback from star formation on the PISN rate using cosmological simulations. We estimate an upper limit of ~ 0.2 PISNe per JWST field of view at any given time. Feedback can reduce this rate significantly, e.g., lowering it to as little as one PISN per 4000 JWST fields of view for the most pessimistic explosion models. We also find that the main obstacle to observing PISNe from the first stars is their scarcity, not their faintness; exposures longer than a few times 10^4 s will do little to increase the number of PISNe found. Given this we suggest a mosaic style search strategy for detecting PISNe from the first stars. Even rather high redshift PISNe are unlikely to be missed by moderate exposures, and a large number of pointings will be required to ensure a detection.

Contents

Acknowledgments	iv
Abstract	v
Chapter 1 Introduction	1
Chapter 2 Pair-Instability Supernovae	6
Chapter 3 JWST Observability	25
Chapter 4 Discussion and Conclusions	36
Chapter 5 Outlook	41
Bibliography	43
Vita	53

Chapter 1

Introduction

The past few decades have revolutionized our understanding of the universe. More precisely, they have made clear exactly how little we understand about the universe, with the realization that the normal baryonic matter we are accustomed to accounts for only 4% of the total energy budget of the universe (Komatsu et al., 2011). Nonetheless, great progress has been made in understanding the formation of the complex structures we see today from the simple initial conditions observed in the cosmic microwave background (CMB). Likewise, vast improvements in our observational abilities, enabled by advances in both technology and technique, allow us to peer ever farther through space and time, viewing galaxies in their infancy. As theory and observations continue to improve, we are rapidly approaching the point of having a complete picture of cosmic history stretching all the way from the simple initial conditions of the early universe to the present epoch.

One of the key challenges in completing this picture will be fully understanding the formation of the first stars and galaxies, as they mark a significant increase in complexity from the primordial universe during the ‘dark ages’ (e.g., Barkana & Loeb 2001; Miralda-Escudé 2003; Bromm et al. 2009; Loeb 2010). These objects initiated a fundamental transformation of the universe, driving both the process of reionization (e.g., Meiksin 2009) and chemical enrichment (e.g., Karlsson et al. 2011). The basic process by which these structures are formed has been fairly well established via the standard Λ CDM model for hierarchical structure formation (e.g., Springel et al. 2005). Within this picture, dark matter halos merge to form progressively larger structures; hence the first stars—and subsequently the first galaxies—form the basic building blocks of present-day galaxies (Bromm & Yoshida, 2011). While the evolution of the dark matter framework within which galaxies evolve has been fairly well established, the complex baryonic physics involved in galaxy formation remains a largely unsolved problem.

As the first galaxies are built up from smaller progenitors hosting the very first stars, these so-called Population III (Pop III) stars have a direct impact on the formation and evolution of all subsequent stages of galaxy formation (e.g., Greif et al. 2010). The basic properties of these Pop III stars have been reasonably well established, with the consensus that the first stars formed in dark matter ‘minihalos’ on the order of $10^5 - 10^6$ solar masses at redshifts $z \simeq 20 - 30$ (Couchman &

Rees, 1986; Haiman et al., 1996; Tegmark et al., 1997). Numerical simulations of the collapse of metal-free gas into these halos, where molecular hydrogen is the only available coolant, had suggested that the first stars were predominantly very massive, with typical masses of $M_* \gtrsim 100 M_\odot$ and a top-heavy initial mass function (IMF) (e.g., Bromm et al. 1999, 2002; Abel et al. 2002; Bromm & Larson 2004; Yoshida et al. 2006; O’Shea & Norman 2007). More recent work has revised this picture, finding that the gas from which the first stars formed underwent significant fragmentation, leading to slightly lower characteristic masses and a much broader IMF than previously thought (Stacy et al., 2010; Clark et al., 2011; Greif et al., 2011).

While the formation of the very first stars is set by cosmological initial conditions, the formation of all subsequent generations is much more complex due to the feedback processes initiated by that very first episode of primordial star formation, including the introduction of metals, and possibly dust and significant magnetic fields. Radiative feedback on the molecular clouds in the first galaxies, supersonic turbulence driven by the process of virialization, cold-flow accretion from the intergalactic medium (IGM), and kinetic and chemical feedback from supernovae will all have an impact on the conditions for star formation in the first galaxies, resulting in a very different mode of star formation from that occurring in cosmological mini-halos. Taking all of these factors into account, state of the art *ab initio* cosmological

simulations have progressed to the formation of $\sim 10^8 M_\odot$ atomic cooling halos collapsing at $z \simeq 10$ (Greif et al., 2010). However, the focus of the next generation of telescopes such as the *James Webb Space Telescope* (JWST), the Atacama Large Millimeter Array (ALMA) and the Giant Magellan Telescope (GMT) will be on systems an order of magnitude larger in size, around $10^9 M_\odot$ (Mashchenko et al., 2008; Pawlik et al., 2011). In order to bridge this gap between theory and observation, it is essential that we understand the effects of this stellar feedback before these next-generation observatories come online.

One key factor in properly modeling galaxy formation is supernova feedback, both through direct mechanical feedback from the explosion itself, and through the chemical enrichment process. For example, it is possible that extremely energetic pair-instability supernovae (PISNe) occurring in low mass minihalos could have contributed substantially to the observed metallicity of the IGM (Bromm et al., 2003; Greif et al., 2007, 2010); however, recent observations of a rapidly declining metal abundance in the IGM above $z \gtrsim 6$ (Becker et al., 2009) make this possibility less likely, and favors a scenario in which enrichment proceeds mainly via delayed galactic outflows at lower redshifts (Kramer et al., 2010). This suggests two possibilities. First, if the majority of the metals produced in PISNe do not escape into the IGM and instead enrich the galaxies into which they are incorporated, those galaxies will be enriched above the critical metallicity for Population II rather than Population

III star formation before the second episode of star formation begins (Greif et al., 2010). Second is the possibility that PISN explosions were the exception rather than the norm, as suggested by recent work lowering the characteristic mass of the first stars (e.g., Greif et al. 2011; Clark et al. 2011). Either way, the ultimate fate of the first stars will have a direct and measurable impact on the observable signatures of the first galaxies. Given this, one key method for constraining the properties of the first galaxies will be the detection and analysis of PISN remnants.

With this in mind, we investigate the ability of the JWST to detect PISNe by estimating their source density and observability. In Chapter 2 we describe our semi-analytic model for the PISN rate. We consider the ability of the JWST to detect PISNe at high redshift in Chapter 3 and our conclusions on the observability of these events are gathered in Chapter 4. In Chapter 5 we present a more general outlook on what remains to be done before first light on the next generation of telescopes, including the JWST, ALMA, and the GMT. Throughout, we adopt a Λ CDM model of hierarchical structure formation, using cosmological parameters consistent with the WMAP 5-year results (Komatsu et al., 2009): $\Omega_{\text{m}} = 0.258$; $\Omega_{\Lambda} = 0.742$; $\Omega_b = 0.0441$; $h = 0.719$; $n_s = 0.96$; $\sigma_8 = 0.796$.

Chapter 2

Pair-Instability Supernovae¹

2.1 The Cosmological Context

Basic one-dimensional models predict that stars with masses in the range 140–260 M_{\odot} will undergo a pair-production instability and explode completely (Barkat et al., 1967; Fraley, 1968). During core oxygen burning, a combination of high temperatures and relatively low densities results in the formation of e^{\pm} pairs, removing pressure support from the core. Following the subsequent contraction, the ignition of explosive oxygen burning completely disrupts the progenitor, resulting in a significant contribution to the metal enrichment of the surrounding medium. More recently, Chatzopoulos & Wheeler (2012) and Yoon et al. (2012) have found that stars with initial masses as low as 65 M_{\odot} can encounter the pair-production

¹This chapter is taken from a paper which has been accepted for publication; a preprint is available as Hummel et al., 2012, ApJ, in press (arXiv:1112.5207v2)

instability if they are rapidly rotating. In this scenario, strong rotationally induced mixing causes nearly homogeneous evolution, such that the star is converted almost entirely to helium before the next phase in its evolution begins. These extremely energetic explosions—approaching 10^{53} ergs for the most massive models—are very luminous, in part due to the large amount of ^{56}Ni produced, and are also very temporally extended as a result of the large mass ejected (Fryer et al., 2001; Heger & Woosley, 2002; Heger et al., 2003; Joggerst & Whalen, 2011; Kasen et al., 2011).

A second possibility for reaching such extreme explosion energies in slightly lower mass stars is the hypernova scenario for rapidly rotating stars that undergo core collapse (Umeda & Nomoto, 2003; Tominaga et al., 2007). During the collapse, accretion onto a central black hole powers a jet which induces a highly energetic explosion. While recent work has decreased the expected mass of the first stars, they have also been found to rotate more rapidly than previously thought (Stacy et al., 2011), increasing the plausibility of this scenario. Evidence supporting this hypothesis has recently been presented by Chiappini et al. (2011).

While not an example of a Pop III star, the recent discovery of the extremely luminous supernova (SN) 2007bi, identified as a possible PISN, in a metal-poor dwarf galaxy at a redshift of $z \simeq 0.1$ (Gal-Yam et al., 2009) suggests that PISNe may be possible in the local universe under rare circumstances. Further supporting this picture, Woosley et al. (2007) have shown that SN 2006gy (Smith et al., 2007) is

well modeled by a pulsational pair-instability model. For stars with initial masses in the range $\sim 100\text{--}140\text{ M}_\odot$, the star encounters the e^\pm production instability, but the resulting explosive ignition of oxygen is insufficient to unbind the star. Instead it ejects a shell of material before settling back into a stable configuration. The star encounters this instability several times until the mass of the helium core drops below $\sim 40\text{ M}_\odot$, after which the star can proceed to silicon burning and eventually undergo core-collapse.

With the upcoming launch of the *James Webb Space Telescope* (JWST) we will be able to probe the epoch of first light in unprecedented detail. While the first stars themselves are unlikely to be visible (e.g, Bromm et al. 2001; Pawlik et al. 2011), some of the SNe that end their lives should be within the detection limits of the JWST (e.g., Mackey et al. 2003; Scannapieco et al. 2005; Gardner et al. 2006). While the basic properties of PISNe and the effect they have on their environment has been well studied (Mori et al., 2002; Bromm et al., 2003; Furlanetto & Loeb, 2003; Kitayama & Yoshida, 2005; Whalen et al., 2008; Wise & Abel, 2008; Greif et al., 2010), the source density of these events has yet to be well constrained.

The first attempt at estimating the number and observability of SNe at high redshift was made by Miralda-Escudé & Rees (1997), who calculated the all-sky SN rate based on estimates of the total metals produced by a typical SN and the observed metallicity of the intergalactic medium (IGM) at high redshifts. This yields

$\sim 1 \text{ SN yr}^{-1} \text{ arcmin}^{-2}$ at $z \sim 5$. Other early work attempted to model the SN rate based on the empirically determined star formation rate out to high redshifts ($z \sim 5$; e.g., Madau et al. 1998; Dahlén & Fransson 1999). It should be noted that these attempts focused on Type II SNe, not PISNe, which are the focus of the present work. Mackey et al. (2003) estimated the PISN rate based on their calculations of the Pop III star formation rate, predicting $\sim 2 \times 10^6 \text{ PISNe yr}^{-1}$ over the whole sky above $z = 15$. Weinmann & Lilly (2005) performed a similar analysis with more conservative estimates for the star formation rate, finding a PISN rate of $\sim 4 \text{ yr}^{-1} \text{ deg}^{-2}$ above $z = 15$ and $\sim 0.2 \text{ yr}^{-1} \text{ deg}^{-2}$ above $z = 25$, as well as concluding that PISNe should be observable up to $z = 50$ with the JWST.

Subsequent work by Wise & Abel (2005) determined the PISN rate based on the collapse of gas into dark matter minihalos. Accounting for radiative feedback, they concluded that $\sim 0.34 \text{ PISNe yr}^{-1} \text{ deg}^{-2}$ were to be expected above $z = 10$, as well as briefly considering the detectability of PISNe at high redshifts based on models from Heger & Woosley (2002). Scannapieco et al. (2005) presented a more thorough analysis of the detectability of PISNe based on a suite of numerical simulations spanning the range of theoretical PISN models using the implicit hydrodynamics code KEPLER. Mesinger et al. (2006b) presented a similar but more general halo mass function based analysis, considering the rates and detectability of all SNe; they briefly consider primordial PISNe, but focus on core-collapse SNe and

their detectability. Most recently, Trenti et al. (2009) explored the observable PISN rate within the context of the metal-free gas supply during the epoch of reionization.

Our work improves upon these investigations by incorporating updated PISN models from Kasen et al. (2011) and determining their observability using the published specifications of the Near Infrared Camera (NIRcam) on the JWST². In the final stages of this work we have become aware of the study by Pan et al. (2012), who have performed a similar analysis. This paper addresses the question of PISN observability in a nicely complementary way by employing a different normalization strategy. Different from our assumption that viable Pop III progenitors can only form in unenriched minihalos at $z \gtrsim 6$, Pan et al. (2012) derive the star formation rates required to produce sufficient photons for reionization. They then infer the PISN rate corresponding to different choices for the IMF. Their analysis is thus able to probe the character of star formation in the dwarf galaxies that are the main drivers of reionization, whereas we focus on the minihalos where Pop III stars first begin to form.

2.2 The PISN Rate

PISNe are produced only by very massive stars (Bromm et al., 2001; Schaerer, 2002; Heger et al., 2003), which are now expected to be rare even for Pop III star formation.

²<http://www.stsci.edu/jwst/instruments/nircam/instrument-design/filters>

After the first massive star forms, the resulting heating from photoionization quickly suppresses the density of the remaining gas in the minihalo, effectively halting star formation (Kitayama et al., 2004; Whalen et al., 2004; Alvarez et al., 2006). The energy released by the first PISN disperses the gas in the halo and contaminates it with metals (Bromm et al., 2003; Greif et al., 2007; Whalen et al., 2008; Wise & Abel, 2008; Greif et al., 2010). Subsequent episodes of star formation are thus delayed until the gas is able to recondense into more massive cosmological halos (Yoshida et al., 2004, 2007; Johnson et al., 2007; Alvarez et al., 2009). While star formation will resume at this point, the gas in these systems is expected to be enriched beyond the critical metallicity for the transition to Pop II star formation (Wise & Abel, 2007, 2008; Greif et al., 2007, 2008, 2010). As a result, the stars that form will no longer be massive enough to reliably produce PISNe. These explosions are thus only expected to occur in minihalos containing pristine gas that has just crossed the density threshold for star formation via H_2 cooling, and only one PISN occurs per halo.

It is possible that the first stars formed in binaries or small multiples; however, the number of massive stars formed per minihalo is still of order unity (Stacy et al., 2010; Clark et al., 2011; Greif et al., 2011). Given this, and assuming that the time required for the progenitor star to form, live and die is negligible (Heger et al., 2003), we can use the formation rate of minihalos to place a robust upper limit on

the PISN rate.

The introduction of cosmic feedback has the potential to significantly alter this picture. Chemical enrichment induces a transition to lower mass Pop II star formation, and thus always has a negative effect on the PISN rate. Radiative feedback—especially H_2 -dissociating Lyman-Werner (LW) feedback—has a more complicated effect. The destruction of molecular hydrogen by LW photons removes the ability of pristine gas to cool effectively. This suppresses star formation, and hence negatively affects the PISN rate. However this merely delays star formation; as the halo mass continues to increase, the gas eventually becomes self-shielding and proceeds with cooling and collapse. The delay effectively increases the amount of gas available when star formation begins. This increases the possibility of multiple massive stars forming simultaneously, positively affecting the PISN rate. To account for these possibilities, we consider three scenarios. First we estimate the PISN rate assuming that the first stars form unimpeded by cosmic feedback. Then we consider a conservative scenario in which both chemical and LW feedback affect the PISN rate, but only one star forms per halo. Finally, we allow for enhanced star formation in the LW-affected halos, and calculate the observable rate for each scenario.

2.2.1 No-Feedback Limit

In order to determine an upper limit to the PISN rate, we assume exactly one PISN per minihalo, forming as soon as the virial temperature of the minihalo exceeds the minimum value T_{crit} required for gas to cool and collapse to high densities. We set this to 2200 K based on the results of simulations (see § 2.2.2 for details). The corresponding critical mass for collapse is given by

$$M_{\text{crit}} = 10^6 \text{ M}_{\odot} \left(\frac{T_{\text{crit}}}{10^3 \text{ K}} \right)^{3/2} \left(\frac{1+z}{10} \right)^{-3/2}, \quad (2.1)$$

where we assume a mean molecular weight of $\mu = 1.22$, appropriate for the almost completely neutral IGM at high redshifts (Barkana & Loeb, 2001).

We use the analytic Press-Schechter (PS) formalism for structure formation (Press & Schechter, 1974) to estimate the number density n_{PS} of minihalos of mass M at redshift z , given by

$$n_{\text{PS}}(M, z) = \sqrt{\frac{2}{\pi}} \frac{\rho_{\text{m}}}{M} \left| \frac{d \ln \sigma_0(M)}{d \ln M} \right| \nu_{c,z} e^{-\nu_{c,z}^2/2}, \quad (2.2)$$

where ρ_{m} is the background matter density, $\sigma_z(M)$ is the standard deviation of overdensities δ of mass M at redshift z , and $\nu_{c,z} = \delta_c / \sigma_z(M)$, where δ_c is the critical overdensity for collapse; the value used here is $\delta_c = 1.686$.

Converting from redshift to cosmic time $t(z)$, where

$$t(z) = \frac{1}{H_0} \int_z^\infty \frac{dz'}{(1+z')\sqrt{\Omega_m(1+z')^3 + \Omega_\Lambda}}, \quad (2.3)$$

a first order estimate for the minihalo formation rate as a function of redshift is given by $\dot{n}_{\text{PS}} \equiv dn_{\text{PS}}/dt$. However, this estimate is only valid while the rate of destruction of minihalos via mergers remains small compared to the formation rate. The Press-Schechter formalism only gives the total number of halos of a given mass at a given redshift. As a result, once mergers become important the rate of change of the total number of minihalos no longer traces the formation rate. To correct for this, we use the expression for the formation rate derived by Sasaki (1994)³:

$$\dot{n}_+(z) = \frac{\dot{D}}{D} n_{\text{PS}}(M_{\text{crit}}, z) \frac{\delta_c^2}{\sigma_0^2(M) D^2}, \quad (2.4)$$

where $D(z)$ is the growth factor. The PISN rate in this upper limit of no feedback, shown in Figure 2.2 (blue line), is then simply given by the halo formation rate:

$$\dot{n}_{\text{PISN}}(z) = \dot{n}_+(z). \quad (2.5)$$

³See Mitra et al. (2011) for a discussion of the validity of this expression.

2.2.2 Feedback

The preceding analysis has only nominally incorporated the baryonic physics involved through the critical mass for H_2 cooling. Gas will not successfully cool and collapse in all minihalos that reach the critical mass (e.g., Yoshida et al. 2003). The various feedback mechanisms responsible for this include photoheating from stars in nearby halos and the buildup of a background of H_2 dissociating LW photons. Chemical feedback will enrich the gas with metals, improving its ability to cool. However, gas that is enriched forms lower-mass Population II stars, effectively reducing the PISN rate. These feedback mechanisms can be represented with distinct efficiency factors $\eta(z)$, such that the true PISN rate will be given by

$$\dot{n}_{\text{PISN}}(z) = \eta_{\text{chem}}(z) \eta_{\text{rad}}(z) \dot{n}_+(z). \quad (2.6)$$

We must include these effects in order to derive a realistic estimate for the PISN rate, which we henceforth refer to as the conservative feedback case.

Lyman-Werner Feedback

LW feedback is of particular importance in any discussion of feedback on the first stars as it dissociates the H_2 molecules primarily responsible for cooling primordial gas. This significantly reduces the ability of the gas to cool and works to suppress further star formation (Haiman et al., 1997; Omukai & Nishi, 1999; Ciardi et al.,

2000; Haiman et al., 2000; Glover & Brand, 2001; Kitayama et al., 2001; Machacek et al., 2001; Ricotti et al., 2001, 2002a,b; Yoshida et al., 2003; Omukai & Yoshii, 2003; Mesinger et al., 2006a). As the first stars form in $\gtrsim 3\sigma$ peaks in the Gaussian distribution of density fluctuations (Barkana & Loeb, 2001), we focus here on a similarly overdense environment in order to provide a conservative estimate of the effects of LW feedback on the PISN rate. While representative of the LW background in Pop III star formation sites, this is likely not representative of the ‘average’ LW background in the universe (e.g., Machacek et al. 2001; Mesinger et al. 2006a).

We will describe our radiative feedback simulations in detail elsewhere, and present only a brief summary here. We employ a set of two cosmological simulations using a modified version of the N -Body/TreePM SPH code GADGET (Springel, 2005; Springel et al., 2001) to gauge the effects of LW feedback on the PISN rate. These simulations, carried out in a box of size $3.125 h^{-1}$ comoving Mpc and starting from a redshift of $z = 127$, were performed to investigate the formation of the first dwarf galaxies in $10^9 M_\odot$ halos at $z = 10$. In order to obtain high resolution in the halo containing the first galaxy while retaining information about structure on large scales, a zoomed simulation technique was used, with the highest resolution dark matter (gas) particles having a mass of 2350 (484) M_\odot . This allows halos with masses $\gtrsim 2 \times 10^5 M_\odot$, to be resolved with $\gtrsim 100$ dark matter particles.

The first of the simulations we employ is similar to simulation *Z4* presented

in Pawlik et al. (2011), and follows the non-equilibrium chemistry and cooling of the primordial atomic and molecular gas, including star formation but not the associated feedback. It thus provides a useful reference against which the effects of LW feedback can be discussed. Here, gas particles were turned stochastically into star particles at densities $n_{\text{H}} > 500 \text{ cm}^{-3}$ on a dynamical time scale. Star particles were considered simple stellar populations using the zero-metallicity top-heavy IMF models from Schaerer (2003). Henceforth this simulation is referred to as Simulation A.

The second simulation employed here, which we refer to as Simulation B, is identical to Simulation A except for the inclusion of LW feedback. Calculation of the feedback was carried out by considering the contribution from both star particles and a uniform LW background. The combined LW background is normalized to approximate the LW background evolution shown in Greif & Bromm (2006) in the optically thin limit, but with the application of a self-shielding correction (Wolcott-Green et al., 2011).

The efficiency of LW feedback, η_{LW} , can be expressed as the ratio of the formation rate of minihalos at the critical mass with LW feedback to that without:

$$\eta_{\text{LW}}(z) = \frac{\dot{n}_{+}(M_{\text{crit,LW}}, z)}{\dot{n}_{+}(M_{\text{crit}}, z)}. \quad (2.7)$$

This requires determining the factor $f_{\text{LW}}(z)$ by which LW feedback increases the critical mass for star formation. We do this by determining the critical mass required

for stars to form in both simulations, as traced by the lowest mass halo that is actively forming stars for the first time. The resulting critical mass in each case is shown in Figure 2.1b; blue points denote the critical mass in Simulation A, red points in Simulation B. Without any negative feedback, we expect stars to form when the halo reaches the critical mass given in Equation 2.1. We find that the resulting critical mass in Simulation A is best fit by a critical virial temperature of 2200 K, as shown in Figure 2.1b. Note that this includes the effects of dynamical heating; gas in isolated halos would collapse and form stars at lower masses.

Determining the critical mass for star formation in the LW feedback simulation in the same manner as above, we can then determine f_{LW} , shown in Figure 2.1a. We find that f_{LW} is well fit by a functional form of

$$f_{\text{LW}}(z) = -6.23 \times 10^{-5} \operatorname{erf}[0.094(z - 0.204)] + 6.23 \times 10^5, \quad (2.8)$$

for $z \geq 10$, where $\operatorname{erf}(z)$ is the error function. $M_{\text{crit,LW}}$ is then given by

$$M_{\text{crit,LW}} = f_{\text{LW}} M_{\text{crit}}, \quad (2.9)$$

shown in Figure 2.1b. When the virial temperature of the halo reaches 10^4 K, cooling via atomic hydrogen becomes efficient and molecular hydrogen becomes unimportant. Once this threshold is reached, LW feedback cannot further suppress star

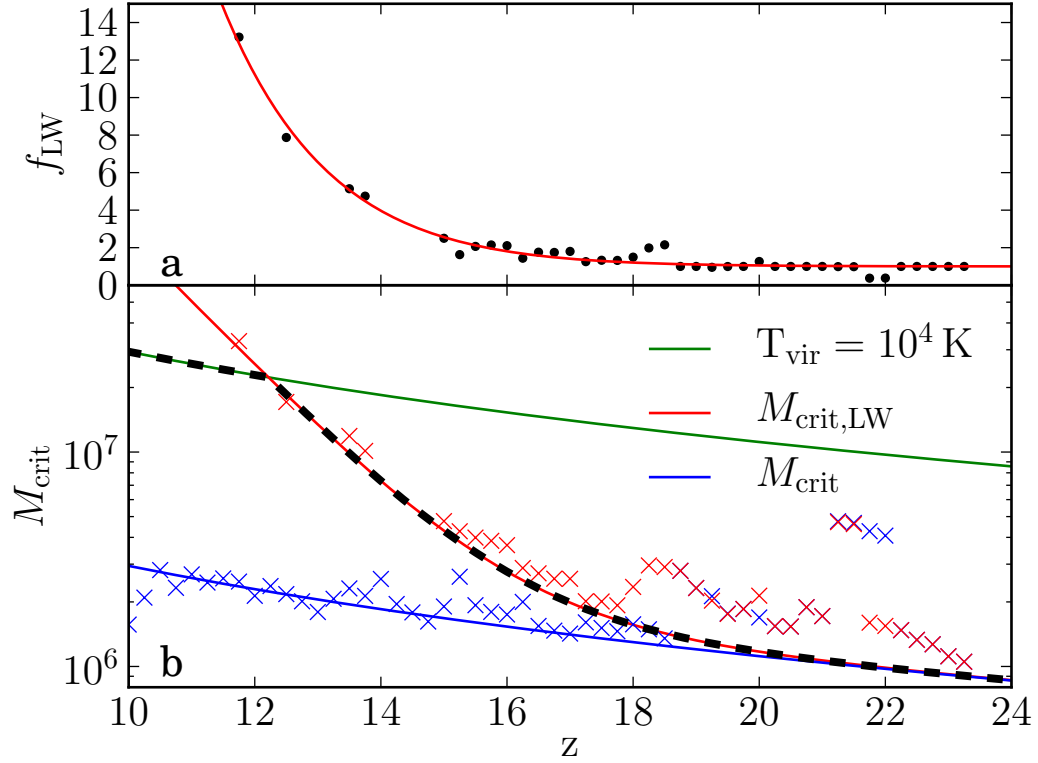


Figure 2.1 Top: the factor f_{LW} by which LW feedback increases the critical mass for star formation; points show the results of the simulation, the red line our fit. Bottom: The critical mass for star formation in both simulations. Blue crosses mark the critical mass for star formation in the absence of LW feedback, red crosses in its presence. The blue line shows the best fit critical mass from Equation 2.1, given by a temperature of 2200 K; the red line the critical mass from Equation 2.9 for LW feedback using the fit for f_{LW} given in Equation 2.8. The black dashed line represents the critical mass employed, accounting for atomic cooling in halos with virial temperatures above 10^4 K.

formation, and $M_{\text{crit,LW}}$ holds steady at a constant virial temperature of 10^4 K. This is reflected as an increase in the formation rate of halos affected only by LW feedback, as the formation rate of atomic cooling halos is increasing prior to $z = 10$. This transition can be clearly seen in Figure 2.2, marked by a sudden jump in the halo formation rate. As ionizing photons cannot easily escape the immediate vicinity of the star that produced them, their impact on neighboring halos is small compared to that of LW photons. We thus set $\eta_{\text{rad}} \simeq \eta_{\text{LW}}$ for simplicity.

Chemical Feedback

The process of chemical enrichment is another crucial factor for determining the PISN rate. Gas that has been enriched beyond a critical metallicity of $Z_{\text{crit}} \sim 10^{-4} Z_{\odot}$ will no longer form Pop III stars (Bromm et al., 2001; Schneider et al., 2002; Bromm & Loeb, 2003), and hence no PISNe. Chemical feedback can thus be represented as the fraction of halos forming from pristine gas at a given redshift. Realistic three-dimensional simulations of this process starting from cosmological initial conditions have become possible in the past decade, showing that enrichment by Pop III SNe, if they are highly energetic, proceeds very inhomogeneously, enriching the IGM before penetrating into denser regions (Scannapieco et al., 2005; Greif et al., 2007; Tornatore et al., 2007; Wise & Abel, 2008; Maio et al., 2010).

In modeling η_{chem} , we use the results of Furlanetto & Loeb (2005). Their

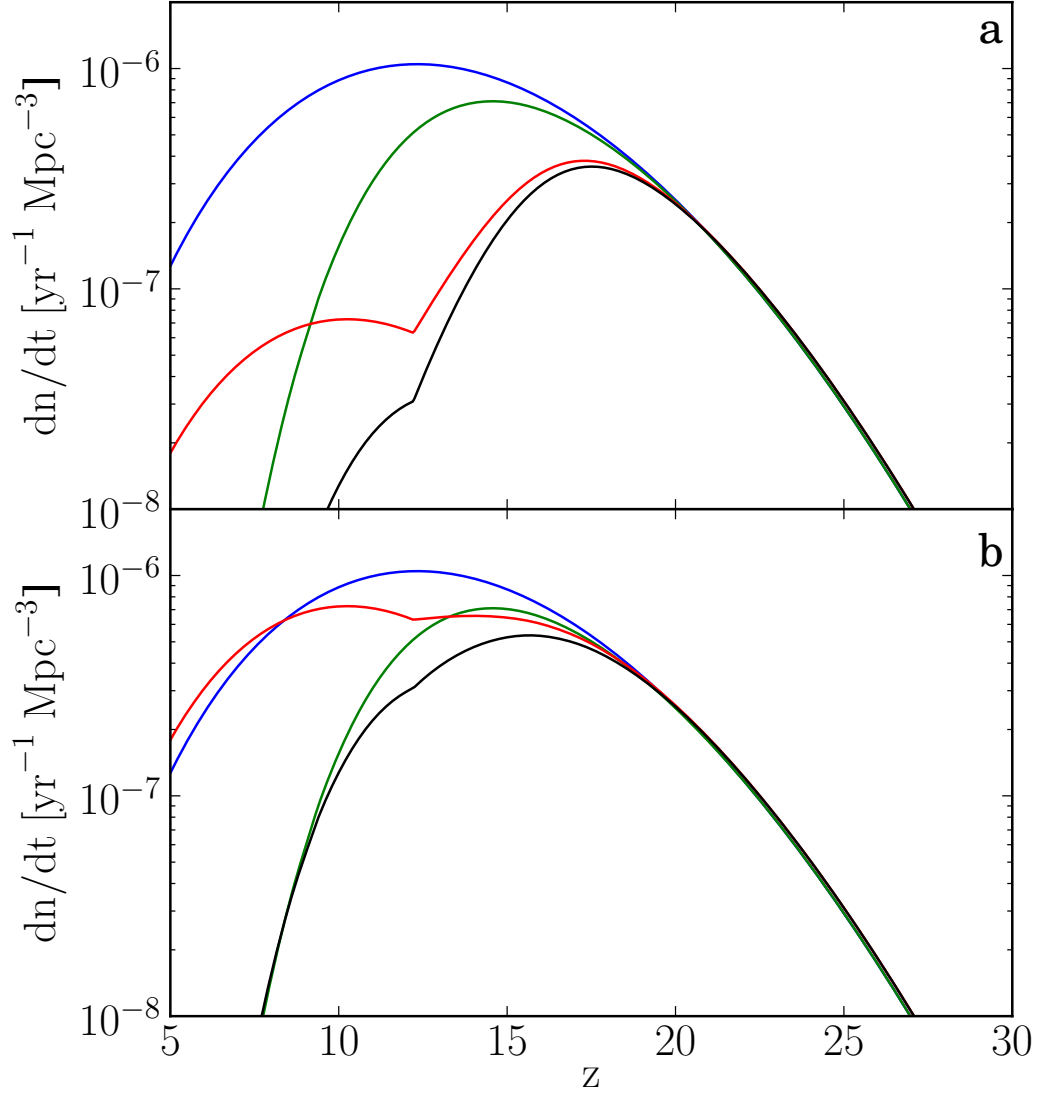


Figure 2.2 a) \dot{n}_{PISN} in the upper limit of no feedback (blue), with chemical feedback (green), LW feedback (red) and the resulting PISN rate for the conservative feedback case (black). b) Same as (a), but for the enhanced star formation case.

semi-analytic treatment of SN winds utilizes the Sedov (1959) solution for an explosion expanding into a uniform medium and yields a probability function $P_{\text{pristine}}(z)$ that the gas in a newly formed halo is pristine. This is plotted in Figure 2 of their paper for various strengths of chemical feedback. We identify this quantity as the fraction of newly collapsed halos that have been polluted with metals, η_{chem} . Given the recent detection of pristine gas at $z = 3$ by Fumagalli et al. (2011), we choose the weakest feedback scenario presented by Furlanetto & Loeb (2005) among the scenarios that incorporate a clustering of sources. The resulting PISN rate is given by the green line in Figure 2.2.

2.2.3 Enhanced Star Formation

Gas cooling and subsequent star formation in halos affected by LW feedback can be delayed until nearly an order of magnitude more gas is available for star formation (Figure 2.1). This increases the likelihood that multiple massive stars form per halo, offsetting the negative effects of LW radiation considered above. We quantify this by positing that the number of PISNe produced per halo at redshift z is given by the ratio of the critical mass in the presence of LW feedback $M_{\text{crit,LW}}$ to the critical mass in the no-feedback case M_{crit} . For example, at $z = 17$, $M_{\text{crit,LW}}/M_{\text{crit}} \approx 1.4$, so for every 10 pristine halos that form, 14 PISNe are produced. In this case the PISN

rate is modified such that

$$\dot{n}_{\text{PISN}}(z) = \frac{M_{\text{crit,LW}}(z)}{M_{\text{crit}}(z)} \eta_{\text{chem}}(z) \eta_{\text{rad}}(z) \dot{n}_+(z). \quad (2.10)$$

The resulting enhanced PISN rate can be seen in Figure 2.2b. In contrast to the conservative feedback case, the net effect of LW feedback is much less significant here, with chemical feedback controlling the final PISN rate.

2.3 The Observable Rate

The observed PISN rate per unit time per unit redshift per unit solid angle is given by

$$\begin{aligned} \frac{dN}{dt_{\text{obs}} dz d\Omega} &= \frac{dN}{dt_{\text{obs}} dV} \frac{dV}{dz d\Omega} \\ &= \frac{1}{(1+z)} \frac{dN}{dt_{\text{em}} dV} r^2 \frac{dr}{dz}. \end{aligned} \quad (2.11)$$

Cosmological time dilation between t_{obs} and t_{em} is accounted for by the $(1+z)$ in the denominator; dV is the comoving volume element and $r(z)$ is the comoving distance to redshift z given by

$$r(z) = \frac{c}{H_0} \int_0^z \frac{dz'}{\sqrt{\Omega_{\text{m}}(1+z')^3 + \Omega_{\Lambda}}}, \quad (2.12)$$

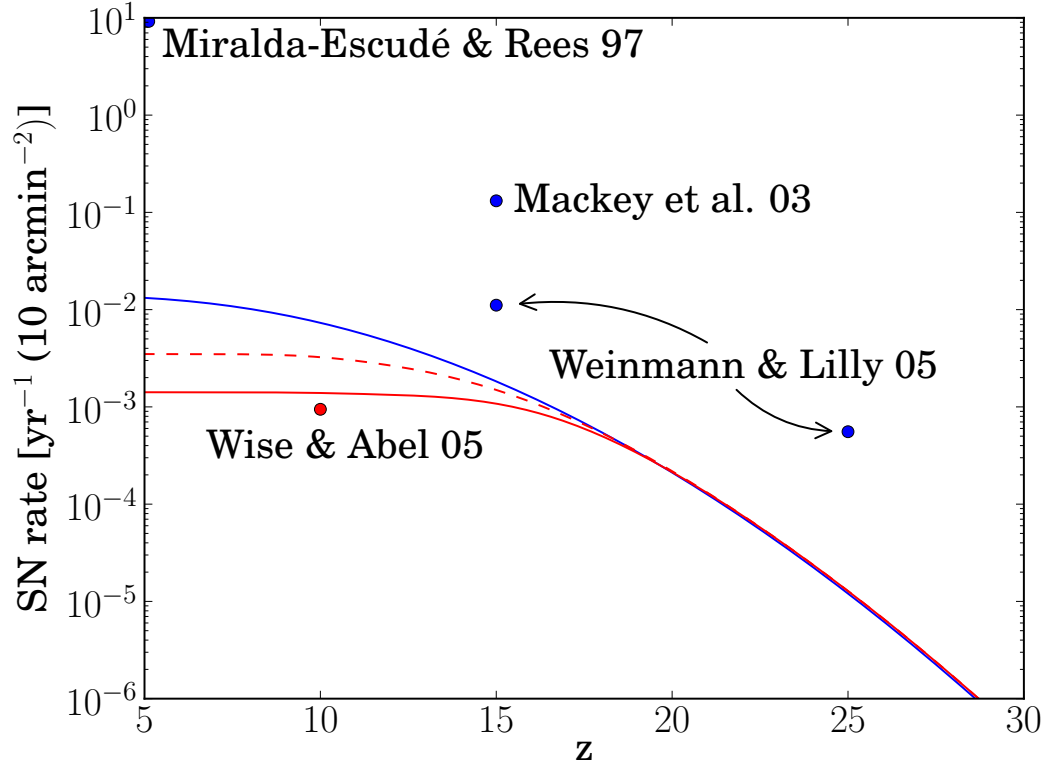


Figure 2.3 The observable PISN rates in number per year per JWST field of view above a given redshift in the upper limit of no feedback (blue line), in the conservative feedback case (solid red line), and the enhanced star formation case (dashed red line). The rates calculated by Miralda-Escudé & Rees (1997), Mackey et al. (2003), Weinmann & Lilly (2005) and Wise & Abel (2005) are also shown for reference. Red points account for feedback; blue points do not.

where c/H_0 is the Hubble distance. With the assumptions outlined above, we estimate the PISN rate in events per year per comoving Mpc^3 in the source rest frame:

$$\frac{dN}{dt_{\text{em}} dV} = \dot{n}_{\text{PISN}}(z), \quad (2.13)$$

such that

$$\frac{dN}{dt_{\text{obs}} dz d\Omega} = \frac{\dot{n}_{\text{PISN}}(z)}{(1+z)} r^2 \frac{dr}{dz}. \quad (2.14)$$

These results—shown in Figure 2.3—are in reasonable agreement with previous work; our no-feedback limit of one PISN per minihalo is somewhat more conservative than that employed by Weinmann & Lilly (2005), but in general agreement. Likewise, our conservative feedback rate is in good agreement with the rate found by Wise & Abel (2005), which also accounted for feedback. The discrepancy with the remaining rates can be attributed to the fact that Mackey et al. (2003) employed an optimistic star formation efficiency of $\eta_* = 0.10$, while Miralda-Escudé & Rees (1997) performed a rough estimate of the all-sky supernova rate based on the observed metallicity of the IGM. This estimate of course includes Pop I and II supernovae in addition to PISNe, and is included only for reference.

Chapter 3

JWST Observability¹

While PISN explosions are predicted to be extremely energetic, the highest redshift events will still be unobservable, and those at lower redshifts will be above the detection limits of the JWST for only a fraction of their lifetimes. To determine the observability of these explosions we must consider both how bright they will be at a given redshift and how long they will remain visible. To span the uncertainties arising from variation in the progenitors of PISNe we consider a set of four models from Kasen et al. (2011), namely their R250, B200, R175 and He100 models. R250 and R175 are red supergiants of $250 M_{\odot}$ and $175 M_{\odot}$, respectively, spanning the mass range of succesful explosions. We also consider a more compact $200 M_{\odot}$ blue supergiant (B200) and a $100 M_{\odot}$ bare helium core (He100). All models considered

¹This chapter is taken from a paper which has been accepted for publication; a preprint is available as Hummel et al., 2012, ApJ, in press (arXiv:1112.5207v2)

here die as PISNe, with explosion energies ranging from 7×10^{52} ergs (R250) to 2×10^{52} ergs (R175). The late-time luminosity is powered by the decay of ^{56}Ni produced during the explosion. $40 M_{\odot}$ of ^{56}Ni are produced in the R250 model, while only 5, 2 and $0.7 M_{\odot}$ are produced in He100, B200 and R175, respectively.

Bare helium cores, such as the He100 model, are of particular interest in light of recent work finding that rapidly rotating stars can encounter the pair-production instability in progenitors with masses as low as $65 M_{\odot}$ (Chatzopoulos & Wheeler, 2012; Yoon et al., 2012). Combined with recent work finding that Pop III stars are both less massive and more rapidly rotating than previously thought (Stacy et al., 2010, 2011, 2012; Clark et al., 2011; Greif et al., 2011, 2012), the explosion of a rapidly rotating helium core formed by homogeneous evolution represents an intriguing possibility.

We first describe our technique for fitting a blackbody to these four PISN models before considering their visibility with the JWST. We then estimate the total observable number in each case and for each feedback prescription. Finally, we briefly discuss the challenges involved in actually identifying PISNe as such.

3.1 A Simple Lightcurve Model

In order to determine how long a PISN will be visible we must model the source spectrum. Given the large mass involved, the ejecta will remain optically thick

until late times, so we make the reasonable assumption that the PISN emits as a blackbody for the majority of its visible lifetime. Using the U, B, V, R, I, J, H, and K absolute magnitude light curves presented in Kasen et al. (2011), we perform a least-squares fit to find the combination of temperature T and radius R_{SN} that best matches the broadband magnitudes at each point in time. This is done with the assumption that the specific luminosity of the PISN $L_{\text{SN},\lambda}$ at wavelength λ is given by

$$L_{\text{SN},\lambda} = 4\pi^2 R_{\text{SN}}^2 B_{\lambda}(T), \quad (3.1)$$

where B_{λ} is the Planck function. The resulting fits for the evolution of the temperature and radius of the PISN models are shown in Figure 3.1. Note that our blackbody assumption breaks down at late times when the photosphere begins to recede into the ejecta. This is manifested as an apparent decrease in the radius of the PISN remnant.

With this information we can then calculate the specific flux $F_{\lambda,\text{em}}$ in the rest frame and—accounting for redshift and cosmological dimming—in the observer’s frame for a source at redshift z :

$$F_{\lambda,\text{obs}}(T, R_{\text{SN}}, z) = \pi \left[\frac{R_{\text{SN}}}{D_L(z)} \right]^2 \frac{B_{\lambda'}(T)}{1+z}. \quad (3.2)$$

Here $\lambda' = \lambda/(1+z)$ accounts for redshifting while the luminosity distance $D_L =$

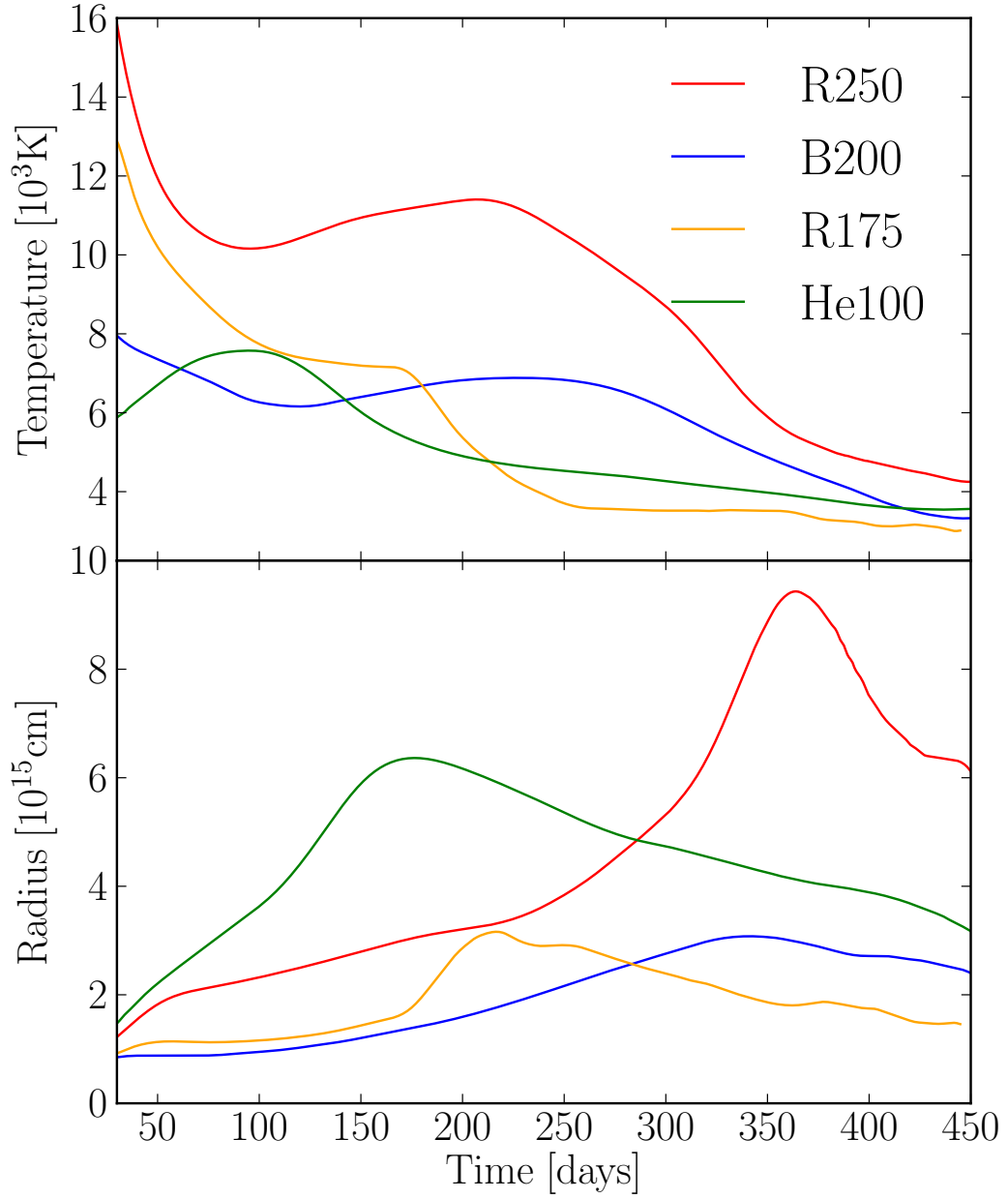


Figure 3.1 The temperature and radius of our blackbody fits as a function of source frame time since the explosion for models R250, B200, R175 and He100. The secondary rise in temperature seen in R250 and B200 is caused by the decay of ^{56}Ni reheating the ejecta at late times. Note also that the apparent radii begin to decrease again at late times; this can be interpreted as the photosphere receding into the ejecta as the material cools.

$(1+z)r(z)$ accounts for cosmological dimming. Convolution of this spectrum with a filter function $\phi_X(\lambda)$ yields the observable flux in filter X:

$$F_{\text{obs},X} = \int_0^\infty \phi_X(\lambda) F_{\lambda,\text{obs}}(T, R_{\text{SN}}, z) d\lambda. \quad (3.3)$$

3.2 Visibility

The NIRCcam instrument on the JWST will observe the early universe through a number of narrow, medium-width, and wide filters². The widest, longest-wavelength filter, F444W, will observe from 3.3 to 5.6 μm with a sensitivity limit of 24.5 nJy required for a 10σ detection in 10^4 seconds (Gardner et al., 2006). Shown in the left-hand column of Figure 3.2 is the observable flux as it would appear in the F444W NIRCcam filter at various redshifts for the most and least easily observable models, R250 and B200, respectively. See Figure 4.1 for why these two were chosen; models He100 and R175 can be found in Figure 3.3. The flux limits for the filter of $4.4 \times 10^{-19} \text{ erg s}^{-1} \text{ cm}^{-2}$ for a 10^6 s exposure and $4.4 \times 10^{-18} \text{ erg s}^{-1} \text{ cm}^{-2}$ for a 10^4 s exposure are also shown for reference. We see that the brightest explosions (R250) would be visible to beyond $z \sim 25$, but are never so bright as to be detectable with current generation telescopes. This is consistent with the non-detection by Frost et al. (2009) in a search of the *Spitzer*/IRAC Dark Field for possible Pop III PISN

²<http://www.stsci.edu/jwst/instruments/nircam/instrument-design/filters>

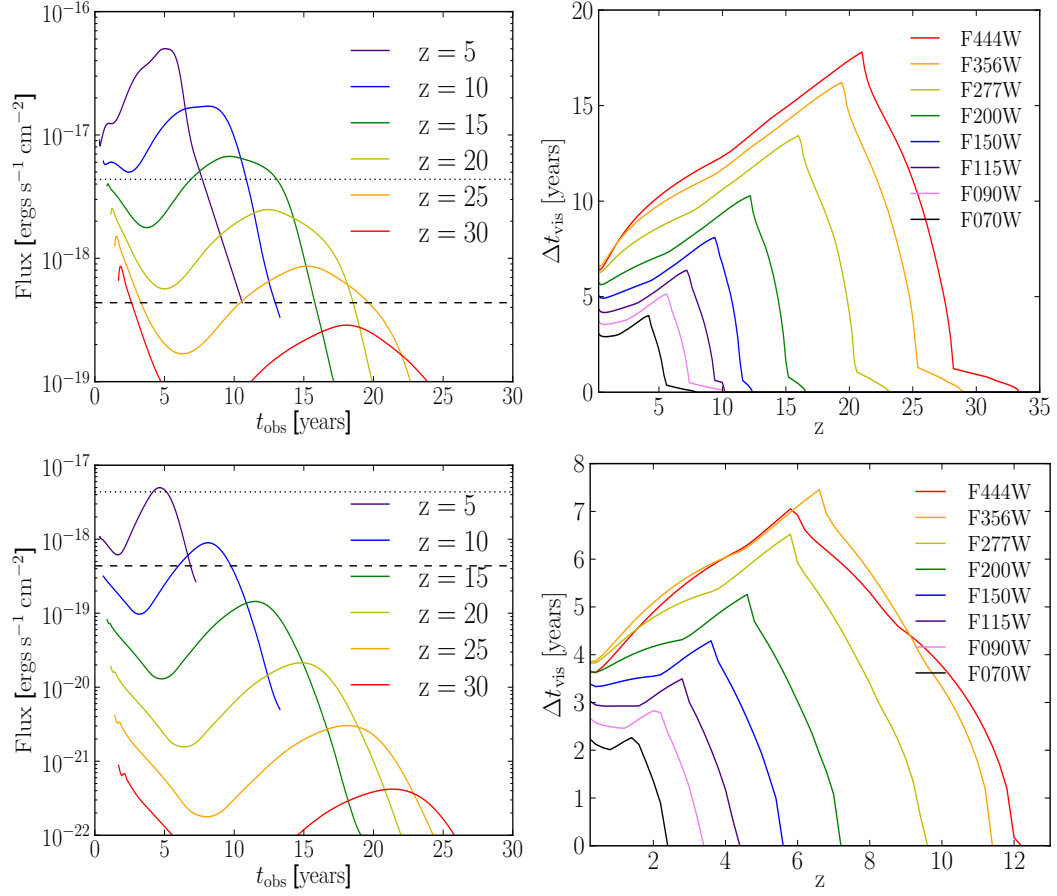


Figure 3.2 Left: Lightcurves for the Kasen et al. (2011) R250 (top) and B200 (bottom) models as they would be observed by JWST’s F444W NIRCam filter at $z = 5, 10, 15, 20, 25$ and 30 . The flux limits for a 10^6 s (dashed line) and 10^4 s (dotted line) exposure are shown for reference. Right: The visibility time Δt_{vis} in years for R250 (top) and B200 (bottom) as a function of redshift for each of the NIRcam wide filters. Note that axes are scaled differently.

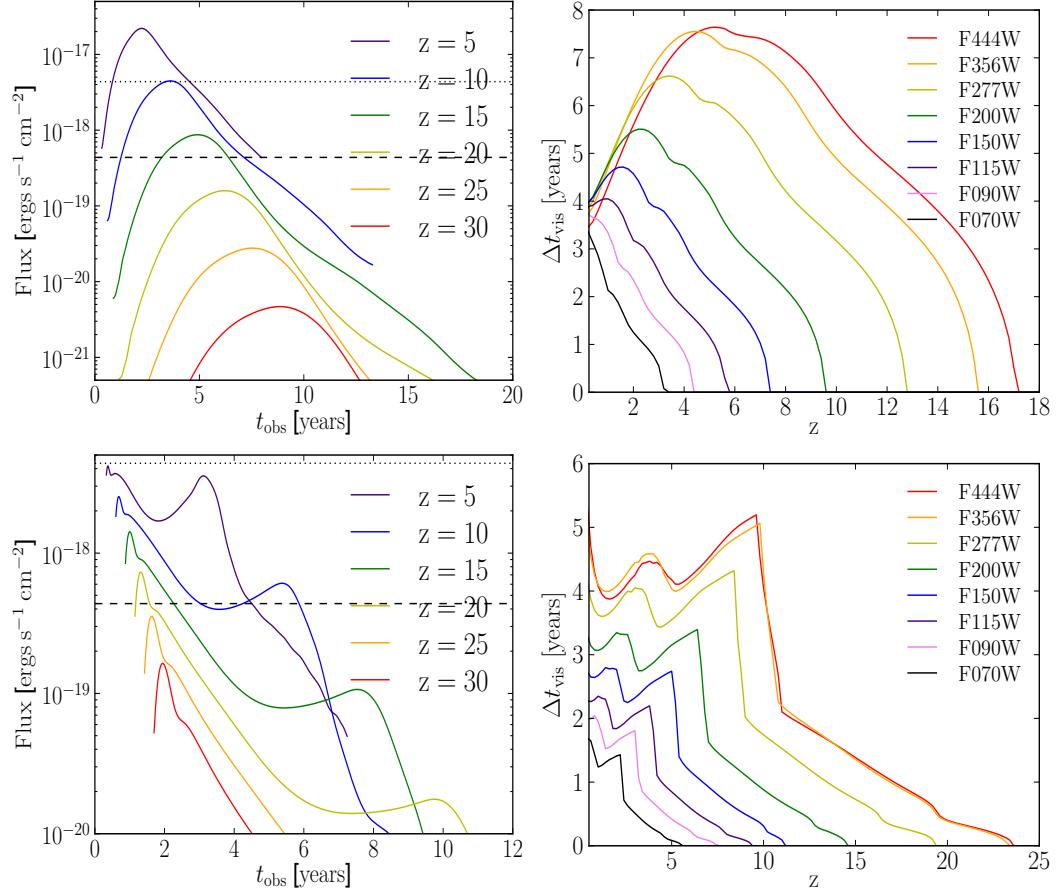


Figure 3.3 Left: Lightcurves for the Kasen et al. (2011) He100 (top) and R175 (bottom) models as they would be observed by JWST’s F444W NIRCam filter at $z = 5, 10, 15, 20, 25$ and 30 . The flux limits for a 10^6 s (dashed line) and 10^4 s (dotted line) exposure are shown for reference. Right: The visibility time Δt_{vis} in years for He100 (top) and R175 (bottom) as a function of redshift for each of the NIRcam wide filters. Note that axes are scaled differently.

candidates.

To account for absorption of flux by neutral hydrogen along the line of sight we implement a simple model of instant reionization at $z = 10$. For sources above this redshift, we assume no flux is observed shortward of the rest frame $\text{Ly}\alpha$ line. This is not relevant for the F444W NIRcam filter as $\text{Ly}\alpha$ does not redshift into the filter until $z \sim 40$, when the lightcurve is already far below even the 10^6 s sensitivity limit. It does however have an effect, albeit a small one, on the F115W and F090W filters.

At low redshifts the duration of the lightcurve presented in Kasen et al. (2011) is not quite long enough for the observed flux to reach the sensitivity limit; we extend it to the limit by extrapolating assuming a power-law scaling. The visible time Δt_{vis} is then simply given by the time the lightcurve is above the filter sensitivity limit. Shown in Figure 3.2 are the visibility times as a function of redshift for each of the NIRcam filters.

3.3 The Observable Number

With this estimate for Δt_{vis} , we may finally calculate the observable number of PISNe on the sky, given by the product of the observed PISN rate at z and the time a PISN at z is visible, Δt_{vis} . This yields an estimate for the number of PISNe

visible on the sky at any given time per unit redshift per unit solid angle:

$$\frac{dN}{dz d\Omega} \simeq \frac{dN}{dt_{\text{obs}} dz d\Omega} \Delta t_{\text{vis}}. \quad (3.4)$$

Figure 3.4 shows the number of PISNe per JWST field of view (FoV) above redshift z in a 10^6 s exposure for all three feedback cases for each PISN model. The results for a 10^4 s exposure are also included for the R250 model only; the other models are not easily observable without deeper exposures.

In the optimistic case of an R250-type PISN with no feedback we expect ~ 0.2 PISNe per JWST FoV for a 10^6 s exposure. In the most pessimistic case of a B200-type PISN with strong negative feedback this number drops to $\sim 2.5 \times 10^{-4}$ per FoV. The actual number detected by the JWST will most likely lie somewhere within this range. Given this, we conclude that a single deep pencil-beam survey is unadvisable for detecting PISNe, as there aren't enough in a given field to ensure a detection, even in the most optimistic upper limit. This suggests that a mosaic search, covering a larger area with shorter exposure times, may be the best approach to ensure finding a Pop III PISN.

3.4 PISN Identification

The exceedingly long duration of their lightcurves poses a serious challenge for identifying PISNe. When combined with the cosmological time dilation factors involved,

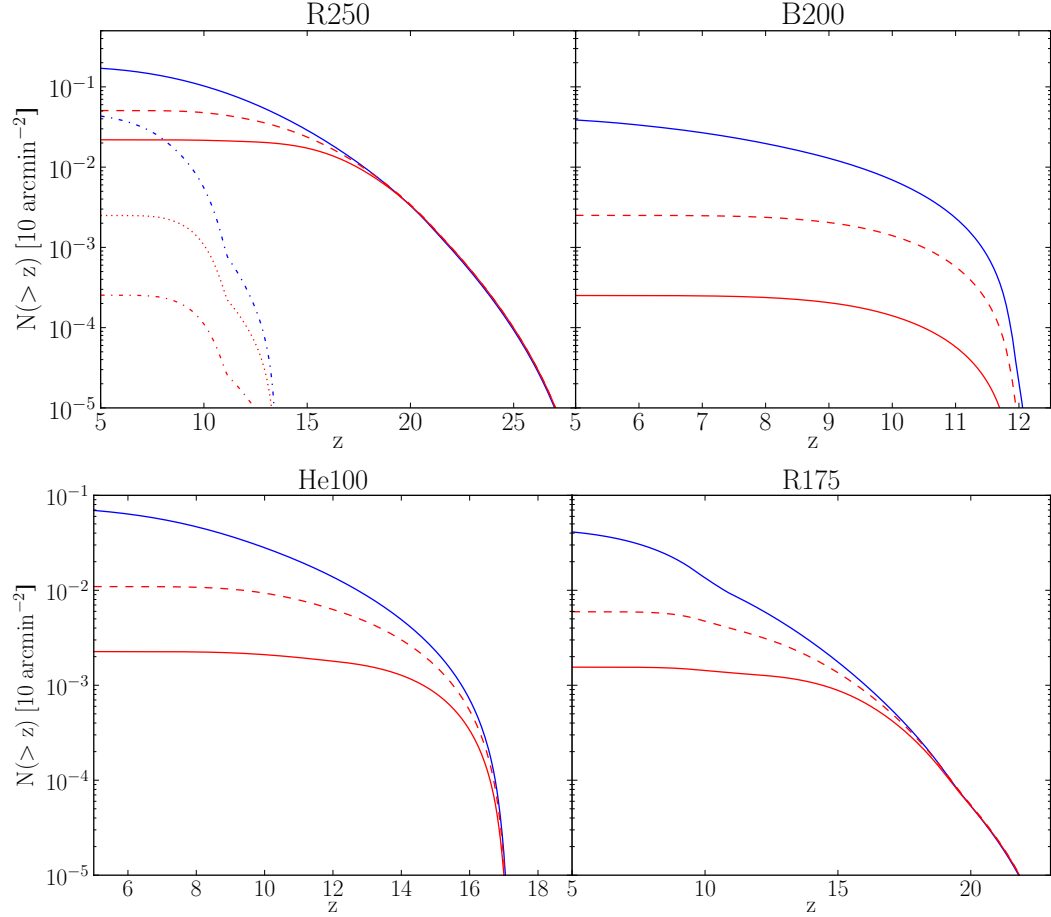


Figure 3.4 Upper and lower limits for the number of PISNe per JWST FoV above redshift z for each PISN model. The observable numbers for a 10^6 s exposure assuming different feedback prescriptions are shown for each model. Solid blue lines show an upper limit to the observable number in the case of no feedback, solid red lines an estimate for the observable number in our conservative feedback scenario, and dashed red lines the number in the enhanced star formation case. Note that the x-axis is scaled differently in each panel. Also shown in the R250 panel are the observable numbers for a 10^4 s exposure for the no-feedback (dot-dashed blue), conservative feedback (dot-dashed red), and enhanced star formation (dotted red) scenarios.

PISN lightcurves can last for decades; the highest redshift events will last longer than the projected mission lifetime for the JWST, making the detection of PISNe by searching for transients difficult at best. However, a multi-year campaign might be able to detect photometric variations; for example, the He100 model would appear to decline in brightness by ~ 0.3 magnitudes per year at redshift $z = 10$ (Kasen et al., 2011). Additionally, PISN colors become redder over time as the photosphere recedes into the ejecta and metal line blanketing suppresses flux in the bluer bands. While likely insufficient to unambiguously identify PISNe, this could be useful in selecting candidates for spectroscopic follow-up.

While the peak bolometric luminosities and spectra of PISNe resemble those of typical Type Ia and Type II supernovae (Joggerst & Whalen, 2011; Kasen et al., 2011), relatively little mixing occurs during the explosion (Joggerst & Whalen, 2011; Chen et al., 2011). As a result, PISNe mostly retain their onion-layer structure during the explosion, and metal lines do not appear in the spectrum until late times when the photosphere has receded deep into the ejecta. Some lighter elements may appear, but the early spectrum of a PISN will be devoid of Si, Ni and Fe lines (Joggerst & Whalen, 2011). This may provide the spectroscopic signature needed to identify PISNe.

Chapter 4

Discussion and Conclusions¹

In this work, we have examined the source density of PISNe from Pop III stars and considered their detectability with the JWST. We conclude that the limiting factor in detecting PISNe will be the scarcity of sources rather than their faintness, in agreement with the conclusions of Weinmann & Lilly (2005). The brightest PISNe should be readily detectable with the longest wavelength NIRcam filters out to $z \sim 25$; the problem is going to be finding one.

We have derived an estimate for the observable PISN rate, finding an upper limit of just over 0.01 PISNe per year per JWST FoV in the case of negligible chemical and radiative feedback. We also find that the inclusion of feedback can reduce the PISN rate by an order of magnitude, to ~ 0.001 per FoV. Accounting

¹This chapter is taken from a paper which has been accepted for publication; a preprint is available as Hummel et al., 2012, ApJ, in press (arXiv:1112.5207v2)

for the possibility of enhanced star formation in halos affected by LW radiation improves this rate slightly, to ~ 0.003 per FoV. The derived PISN rate then allows us to place an upper limit on the observable number of PISNe in a 10^6 s exposure of ~ 0.2 PISNe per JWST FoV in the no-feedback case. The most pessimistic case of a B200-type PISN with strong negative feedback reduces this number to $\sim 2.5 \times 10^{-4}$ per FoV, or one PISN per 4000 JWST fields of view.

The long duration of PISN lightcurves imply that spectroscopic follow-up of PISNe will likely be of great importance. PISN lightcurves can last for decades when combined with the cosmological time dilation factors at high redshifts, making the detection of PISNe by looking for transients untenable. However, a multi-year campaign could identify candidates photometrically, and the lack of metal lines in the spectrum at early times could provide a spectroscopic signature for identification.

We find that the main obstacle to observing PISNe is the paucity of sources. Beyond a moderate exposure time of a few times 10^4 s, the observability of bright PISNe is not a strong function of exposure time and is instead controlled by the source density; this is evident from Figure 4.1, where we have shown the number of JWST FoVs required to detect 10 PISNe (blue) as a function of exposure time for each of our PISN models. The upper boundaries correspond to our conservative estimate for the PISN rate in the presence of feedback, and the lower limits to

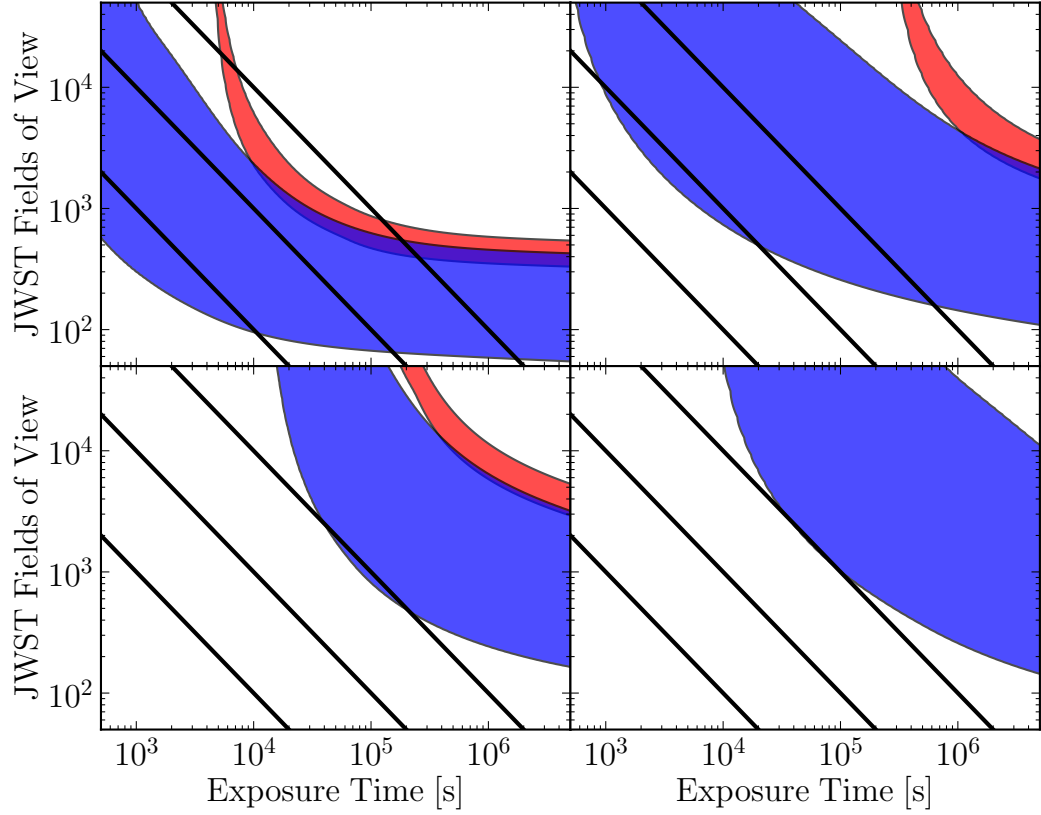


Figure 4.1 The observability of the R250, He100, B200, and R175 models (clockwise from upper left) from Kasen et al. (2011) using the JWST’s NIRcam F444W filter. Shown is the possible range for the number of JWST FoVs required to detect 10 sources as a function of exposure time. The blue range is for all PISNe, and the red for PISNe from $z > 15$. The lower boundaries correspond to the no-feedback upper limit to the PISN rate and the upper boundaries to the conservative feedback rate. From left to right, the black lines represent the number of pointings possible in a total of 10^6 , 10^7 , and 10^8 s for a given exposure time.

the estimated rate without feedback. We can see that the decrease in the required number of JWST pointings slows considerably beyond $\sim 10^5$ s, hence a deep pencil-beam survey would not be advisable in searching for PISNe. Even for only high-redshift sources ($z > 15$; red) the dependence on exposure time is still minimal, being controlled by the lack of sources once the required imaging depth is reached.

Of particular interest in Figure 4.1 are the black lines representing the total number of pointings possible in 10^6 , 10^7 , and 10^8 s for a given exposure time and their location relative to the observability ranges in blue and red. 10^6 s is approximately the limit of what would be possible with a dedicated deep-field campaign; 10^7 s is the limit of the observations the JWST could make in a year assuming NIRCам is in use one third of the time; 10^8 s (~ 10 years) is the projected mission lifetime.

While the detection of a PISN from a ‘first’ star at very high redshifts would be exciting and is in fact possible given the detection limits of the JWST, the scarcity of sources at these redshifts means that such a detection would be highly contingent on serendipity. Even in the most optimistic case, with all available minihalos producing an R250-type PISN, the observability range for such events lies well above what is possible even in a full year of observations, though a few may be detected over the lifetime of the telescope. The detection of a PISN at lower redshifts appears to be more realistic. As the faintest PISNe (R175 and B200) are effectively unobservable, PISN searches should focus on looking for PISNe similar to the R250

and He100 models. In this case, the strategy with the highest likelihood of detection will be a mosaic survey of many moderately deep exposures, possibly similar to the ongoing Brightest of Reionizing Galaxies survey with the *Hubble Space Telescope* (Trenti et al., 2011; Bradley et al., 2012).

Chapter 5

Outlook

With the launch of the JWST we will be able to probe the epoch of first light and reionization for the first time. While we will not be able to probe the entire history of the universe, we will be able to match *ab initio* theoretical predictions to observations at high redshifts and thus construct a complete physical history of the universe from the Big Bang to the present. The detection of PISNe from Pop III stars will play a vital role in deciphering these observations, as they will provide the only direct observational constraints on the stars that ended the dark ages.

Understanding the properties of these first stars is crucial, as the feedback processes they initiate greatly increase the complexity of all subsequent episodes of star formation. If a significant fraction of the first stars explode as PISNe as expected, the formation of the next generation could be delayed for up to 10^7 years, a significant fraction of the Hubble time at such redshifts (Johnson et al., 2007;

Yoshida et al., 2007; Whalen et al., 2008). Regardless of their mass, however, the first stars will doubtless introduce a number of factors driving increased complexity within the first galaxies, including the introduction of metals, and possibly dust and significant magnetic fields. Radiative feedback on the molecular clouds in the first galaxies and supersonic turbulence driven by the process of virialization will also have an impact on the conditions for star formation in the first galaxies, resulting in a possibly very different mode of star formation from that experienced by stars forming in cosmological minihalos.

Current observations are beginning to hint at what we might find. Galaxies at $z \sim 7$ appear to be quite compact, with an average size of 0.7 ± 0.3 kpc (Oesch et al., 2010). These high-redshift galaxies also appear to be quite blue, with a hard UV continuum, and the lower the luminosity of the system, the bluer it is (Bouwens et al., 2010a,b; Finkelstein et al., 2010). This suggests extremely low metallicities, and is consistent with a top-heavy IMF.

Though these observations would seem to suggest we are headed in the right direction, much work remains to be done. While numerical simulations performed during the previous decade had suggested that the first stars were very massive, with $M_* \gtrsim 100 M_\odot$ and a top-heavy IMF, more recent work has found that the protostellar disks from which the first stars formed underwent significant fragmentation (Stacy et al., 2010; Clark et al., 2011; Greif et al., 2011). These results have

initiated a paradigm change in our understanding of Pop III star formation, with slightly lower characteristic masses and a much broader IMF now expected. However, these systems are just on the verge of being gravitationally unstable, and the introduction of external sources of heat could cause the accretion disk to remain rotationally supported. This would then allow for the formation of very massive Pop III stars after all.

In future work we therefore plan to investigate heating via cosmic rays produced in primordial supernovae as one possible avenue for keeping the disk gravitationally stable. we will perform cosmological simulations using the smoothed particle hydrodynamics (SPH) code GADGET to study the formation of the first stars with high resolution, implementing the prescriptions for cosmic ray heating and ionization developed by Stacy & Bromm (2007). Such studies will help us to further understand the nuances of primordial star formation and the effects of supernova feedback on that process, as well as leading towards the ultimate goal of predicting the observational signature of the first galaxies.

Bibliography

- Abel, T., Bryan, G. L., & Norman, M. L. 2002, *Science*, 295, 93
- Alvarez, M. A., Bromm, V., & Shapiro, P. R. 2006, *ApJ*, 639, 621
- Alvarez, M. A., Wise, J. H., & Abel, T. 2009, *ApJ*, 701, L133
- Barkana, R., & Loeb, A. 2001, *Phys. Rep.*, 349, 125
- Barkat, Z., Rakavy, G., & Sack, N. 1967, *Phys. Rev. Lett.*, 18, 379
- Becker, G. D., Rauch, M., & Sargent, W. L. W. 2009, *ApJ*, 698, 1010
- Bouwens, R. J., et al. 2010a, *ApJ*, 709, L133
- . 2010b, *ApJ*, 708, L69
- Bradley, L. D., et al. 2012, *ApJ*, submitted (arXiv:1204.3641)
- Bromm, V., Coppi, P. S., & Larson, R. B. 1999, *ApJ*, 527, L5
- . 2002, *ApJ*, 564, 23

- Bromm, V., Kudritzki, R. P., & Loeb, A. 2001, *ApJ*, 552, 464
- Bromm, V., & Larson, R. B. 2004, *ARA&A*, 42, 79
- Bromm, V., & Loeb, A. 2003, *Nature*, 425, 812
- Bromm, V., & Yoshida, N. 2011, *ARA&A*, 49, 373
- Bromm, V., Yoshida, N., & Hernquist, L. 2003, *ApJ*, 596, L135
- Bromm, V., Yoshida, N., Hernquist, L., & McKee, C. F. 2009, *Nature*, 459, 49
- Chatzopoulos, E., & Wheeler, J. C. 2012, *ApJ*
- Chen, K.-J., Heger, A., & Almgren, A. S. 2011, *Comp. Phys. Communications*, 182, 254
- Chiappini, C., Frischknecht, U., Meynet, G., Hirschi, R., Barbuy, B., Pignatari, M., Decressin, T., & Maeder, A. 2011, *Nature*, 472, 454
- Ciardi, B., Ferrara, A., & Abel, T. 2000, *ApJ*, 533, 594
- Clark, P. C., Glover, S. C. O., Smith, R. J., Greif, T. H., Klessen, R. S., & Bromm, V. 2011, *Science*, 331, 1040
- Couchman, H. M. P., & Rees, M. J. 1986, *MNRAS*, 221, 53
- Dahlén, T., & Fransson, C. 1999, *A&A*, 350, 349

- Finkelstein, S. L., Papovich, C., Giavalisco, M., Reddy, N. A., Ferguson, H. C., Koekemoer, A. M., & Dickinson, M. 2010, *ApJ*, 719, 1250
- Fraley, G. S. 1968, *Ap&SS*, 2, 96
- Frost, M. I., Surace, J., Moustakas, L. A., & Krick, J. 2009, *ApJ*, 698, L68
- Fryer, C. L., Woosley, S. E., & Heger, A. 2001, *ApJ*, 550, 372
- Fumagalli, M., O’Meara, J. M., & Prochaska, J. X. 2011, *Science*, 334, 1245
- Furlanetto, S. R., & Loeb, A. 2003, *ApJ*, 588, 18
- . 2005, *ApJ*, 634, 1
- Gal-Yam, A., et al. 2009, *Nature*, 462, 624
- Gardner, J. P., et al. 2006, *Space Sci. Rev.*, 123, 485
- Glover, S. C. O., & Brand, P. W. J. L. 2001, *MNRAS*, 321, 385
- Greif, T. H., & Bromm, V. 2006, *MNRAS*, 373, 128
- Greif, T. H., Bromm, V., Clark, P. C., Glover, S. C. O., Smith, R. J., Klessen, R. S., Yoshida, N., & Springel, V. 2012, *MNRAS*, submitted (arXiv:1202.5552), 17
- Greif, T. H., Glover, S. C. O., Bromm, V., & Klessen, R. S. 2010, *ApJ*, 716, 510
- Greif, T. H., Johnson, J. L., Bromm, V., & Klessen, R. S. 2007, *ApJ*, 670, 1

- Greif, T. H., Johnson, J. L., Klessen, R. S., & Bromm, V. 2008, MNRAS, 387, 1021
- Greif, T. H., Springel, V., White, S. D. M., Glover, S. C. O., Clark, P. C., Smith, R. J., Klessen, R. S., & Bromm, V. 2011, ApJ, 737, 75
- Haiman, Z., Abel, T., & Rees, M. J. 2000, ApJ, 534, 11
- Haiman, Z., Rees, M. J., & Loeb, A. 1997, ApJ, 476, 458
- Haiman, Z., Thoul, A. A., & Loeb, A. 1996, ApJ, 464, 523
- Heger, A., Fryer, C. L., Woosley, S. E., Langer, N., & Hartmann, D. H. 2003, ApJ, 591, 288
- Heger, A., & Woosley, S. E. 2002, ApJ, 567, 532
- Joggerst, C. C., & Whalen, D. J. 2011, ApJ, 728, 129
- Johnson, J. L., Greif, T. H., & Bromm, V. 2007, ApJ, 665, 85
- Karlsson, T., Bromm, V., & Bland-Hawthorn, J. 2011, Rev. Mod. Phys., submitted (arXiv:1101.4024)
- Kasen, D., Woosley, S. E., & Heger, A. 2011, ApJ, 734, 102
- Kitayama, T., Susa, H., Umemura, M., & Ikeuchi, S. 2001, MNRAS, 326, 1353
- Kitayama, T., & Yoshida, N. 2005, ApJ, 630, 675

- Kitayama, T., Yoshida, N., Susa, H., & Umemura, M. 2004, *ApJ*, 613, 631
- Komatsu, E., et al. 2009, *ApJS*, 180, 330
- . 2011, *ApJS*, 192, 18
- Kramer, R. H., Haiman, Z., & Madau, P. 2010, *MNRAS*, submitted
(arXiv:1007.3581)
- Loeb, A. 2010, *How Did the First Stars and Galaxies Form?* (Princeton University Press)
- Machacek, M. E., Bryan, G. L., & Abel, T. 2001, *ApJ*, 548, 509
- Mackey, J., Bromm, V., & Hernquist, L. 2003, *ApJ*, 586, 1
- Madau, P., Della Valle, M., & Panagia, N. 1998, *MNRAS*, 297, L17
- Maio, U., Ciardi, B., Dolag, K., Tornatore, L., & Khochfar, S. 2010, *MNRAS*, 407, 1003
- Mashchenko, S., Wadsley, J., & Couchman, H. M. P. 2008, *Science*, 319, 174
- Meiksin, A. 2009, *Rev. Mod. Phys.*, 81, 1405
- Mesinger, A., Bryan, G. L., & Haiman, Z. 2006a, *ApJ*, 648, 835
- Mesinger, A., Johnson, B. D., & Haiman, Z. 2006b, *ApJ*, 637, 80

- Miralda-Escudé, J. 2003, *Science*, 300, 1904
- Miralda-Escudé, J., & Rees, M. J. 1997, *ApJ*, 478, 57
- Mitra, S., Kulkarni, G., Bagla, J. S., & Yadav, J. K. 2011, *Bull. Astr. Soc. of India*, 39, 563
- Mori, M., Ferrara, A., & Madau, P. 2002, *ApJ*, 571, 40
- Oesch, P. A., et al. 2010, *ApJ*, 709, L21
- Omukai, K., & Nishi, R. 1999, *ApJ*, 518, 64
- Omukai, K., & Yoshii, Y. 2003, *ApJ*, 599, 746
- O’Shea, B. W., & Norman, M. L. 2007, *ApJ*, 654, 66
- Pan, T., Kasen, D., & Loeb, A. 2012, *MNRAS*, 2809
- Pawlik, A. H., Milosavljević, M., & Bromm, V. 2011, *ApJ*, 731, 54
- Press, W. H., & Schechter, P. 1974, *ApJ*, 187, 425
- Ricotti, M., Gnedin, N. Y., & Shull, J. M. 2001, *ApJ*, 560, 580
- . 2002a, *ApJ*, 575, 33
- . 2002b, *ApJ*, 575, 49
- Sasaki, S. 1994, *PASJ*, 46, 427

- Scannapieco, E., Madau, P., Woosley, S. E., Heger, A., & Ferrara, A. 2005, *ApJ*, 633, 1031
- Schaerer, D. 2002, *A&A*, 382, 28
- . 2003, *A&A*, 397, 527
- Schneider, R., Ferrara, A., Natarajan, P., & Omukai, K. 2002, *ApJ*, 571, 30
- Sedov, L. I. 1959, *Similarity and Dimensional Methods in Mechanics*
- Smith, N., et al. 2007, *ApJ*, 666, 1116
- Springel, V. 2005, *MNRAS*, 364, 1105
- Springel, V., White, S. D. M., Tormen, G., & Kauffmann, G. 2001, *MNRAS*, 328, 726
- Springel, V., et al. 2005, *Nature*, 435, 629
- Stacy, A., & Bromm, V. 2007, *MNRAS*, 382, 229
- Stacy, A., Bromm, V., & Loeb, A. 2011, *MNRAS*, 413, 543
- Stacy, A., Greif, T. H., & Bromm, V. 2010, *MNRAS*, 403, 45
- . 2012, *MNRAS*, 422, 290

- Tegmark, M., Silk, J., Rees, M. J., Blanchard, A., Abel, T., & Palla, F. 1997, *ApJ*, 474
- Tominaga, N., Umeda, H., & Nomoto, K. 2007, *ApJ*, 660, 516
- Tornatore, L., Ferrara, A., & Schneider, R. 2007, *MNRAS*, 382, 945
- Trenti, M., Stiavelli, M., & Michael Shull, J. 2009, *ApJ*, 700, 1672
- Trenti, M., et al. 2011, *ApJ*, 727, L39
- Umeda, H., & Nomoto, K. 2003, *Nature*, 422, 871
- Weinmann, S. M., & Lilly, S. J. 2005, *ApJ*, 624, 526
- Whalen, D., Abel, T., & Norman, M. L. 2004, *ApJ*, 610, 14
- Whalen, D. J., van Veelen, B., O’Shea, B. W., & Norman, M. L. 2008, *ApJ*, 682, 49
- Wise, J. H., & Abel, T. 2005, *ApJ*, 629, 615
- . 2007, *ApJ*, 665, 899
- . 2008, *ApJ*, 685, 40
- Wolcott-Green, J., Haiman, Z., & Bryan, G. L. 2011, *MNRAS*, 418, 838
- Woosley, S. E., Blinnikov, S., & Heger, A. 2007, *Nature*, 450, 390
- Yoon, S.-C., Dierks, A., & Langer, N. 2012, *A&A*, submitted (arXiv:1201.2364)

Yoshida, N., Abel, T., Hernquist, L., & Sugiyama, N. 2003, ApJ, 592, 645

Yoshida, N., Bromm, V., & Hernquist, L. 2004, ApJ, 605, 579

Yoshida, N., Oh, S. P., Kitayama, T., & Hernquist, L. 2007, ApJ, 663, 687

Yoshida, N., Omukai, K., Hernquist, L., & Abel, T. 2006, ApJ, 652, 6

Vita

Jacob Hummel was born in St. Louis, Missouri, the son of John and Catherine Hummel. After graduating from Helias High School, Jefferson City, Missouri in 2005, he entered Truman State University in Kirksville, Missouri. He graduated Valedictorian, receiving the degree of Bachelor of Science in May of 2009. In August of 2009 he entered The Graduate School at The University of Texas at Austin, where he is currently working towards his PhD.

Permanent Address: jacob.a.hummel@gmail.com

This thesis was typeset with $\text{\LaTeX 2}_{\varepsilon}$ ¹ by the author.

¹ $\text{\LaTeX 2}_{\varepsilon}$ is an extension of \LaTeX . \LaTeX is a collection of macros for \TeX . \TeX is a trademark of the American Mathematical Society. The macros used in formatting this thesis were written by Dinesh Das, Department of Computer Sciences, The University of Texas at Austin, and extended by Bert Kay, James A. Bednar, and Ayman El-Khashab.